SCANNING VOL. 32, 49–59 (2010)
© Wiley Periodicals, Inc.

Self-Leveling Two-Dimensional Probe Arrays for Dip Pen Nanolithography®

JASON HAAHEIM, VADIM VAL, JOHN BUSSAN, SERGEY ROZHOK, JAE-WON JANG, JOE FRAGALA, AND MIKE NELSON

NanoInk, Inc., Skokie, Illinois

Summary: Scanning probe lithography (SPL) has witnessed a dramatic transformation with the advent of two-dimensional (2D) probe arrays. Although early work with single probes was justifiably assessed as being too slow to practically apply in a nanomanufacturing context, we have recently demonstrated throughputs up to $3 \times 10^7\,\mu m^2/h$—in some cases exceeding e-beam lithography—using centimeter square arrays of 55,000 tips tailored for Dip Pen Nanolithography® (DPN®). Parallelizing DPN has been critical because there exists a need for a lithographic process that is not only high throughput, but also high resolution (DPN has shown line widths down to 14 nm) with massive multiplexing capabilities. Although previous methods required non-trivial user manipulation to bring the 2D array level to the substrate, we now demonstrate a self-leveling fixture for NanoInk's 2D nano PrintArray. When mounted on NanoInk's NLP 2000, the 55,000 tip array can achieve a planarity of $<0.1^\circ$ with respect to the substrate in a matter of seconds, with no user manipulation required. Additional fine-leveling routines (<2 min of user interaction) can improve this planarity to $<0.002^\circ$ with respect to the substrate—a Z-difference of less than 600 nm across $1\,cm^2$ of surface area. We herein show highly homogeneous etch-resist nanostructure results patterned from a self-leveled array of DPN pens, with feature size standard deviation of $<6\%$ across a centimeter square sample. We illustrate the mechanisms and methods of the self-leveling fixture, and detail the advantages thereof. Finally, we emphasize that this methodology brings us closer to the goal of true nanomanufacturing by automating the leveling process, reducing setup time by at least a factor of 10, enhancing the ease of the overall printing process, and ultimately ensuring a more level device with subsequently homogeneous nanostructures. SCANNING 32: 49–59, 2010. © 2010 Wiley Periodicals, Inc.

Key words: Dip Pen Nanolithography®, DPN®, alkanethiols, gold, nanofabrication, atomic force microscope, AFM, scanning probe lithography, SPL, nanolithography, scanning probe microscopy, SPM, nanoscale lithography, nanoscale deposition, direct deposition, leveling automation, microscale device planarity, massively parallel nanopatterning, 2D cantilever arrays, 2D tip arrays

Introduction

Dip Pen Nanolithography® (DPN® NanoInK, Stokie, IL) is a direct write scanning probe-based technique which operates under ambient conditions, making it suitable to deposit a wide range of biological and inorganic materials. Precision nanoscale deposition is a fundamental requirement to advance nanoscale technology in commercial applications, and tailoring chemical composition and surface structure on the sub-100-nm scale benefits researchers in areas ranging from cell adhesion to biological recognition, cell-signaling, nanoassays, and biomimetic membranes. DPN's basis as a scanning probe technique confers the unique ability of directed placement—materials of interest can be placed exactly (and only) where desired, and fabricated patterns can be immediately verified by atomic force microscopy (AFM). Relative to other related micro/nano patterning techniques (e.g., microcontact printing, e-beam lithography (EBL), nanoimprint lithography, microspotting, or ink-jet printing), this directed placement capability singularly provides the ability register to existing features, or register multiple layers of DPN-printed features

Address for reprints: Jason Haaheim, NanoInk, Inc: 8025 Lamon Avenue, Skokie, IL 60077
E-mail: jhaaheim@nanoink.net

Received 21 January 2010; Accepted with revision 11 February 2010

DOI 10.1002/sca.20175
Published online 31 March 2010 in Wiley InterScience (www.interscience.wiley.com)

to themselves (Haaheim *et al*. 2005; Haaheim and Nafday 2008; Nafday *et al*. 2009).

Since its inception in 1999 (Piner *et al*. 1999), DPN has evolved significantly from the single-tip technique that patterned alkane thiols on gold. Early work involved expanding the usable palette of inks to include DNA (Demers *et al*. 2001, 2002), proteins (Lee *et al*. 2002, 2003), polymers such as polyethylene glycol (Sanedrin *et al*. 2008), and conductive silver nanoparticle solutions (Wang *et al*. 2008). (A comprehensive discussion of the wide variety of published DPN inks can be found in several recent review articles: Ginger *et al*. 2004; Haaheim and Nafday 2008; Huck 2007; Lenhert 2008; Rosner and Demers 2005; Salaita *et al*. 2007.) DPN is high resolution, patterning 14-nm line widths at 20 nm pitches (Haaheim *et al*. 2005), and it is the only sub-50-nm technique that can directly deposit molecules under ambient conditions. Importantly, DPN has been shown to function as both a bottom-up approach (i.e., templating) and a to-down approach (i.e., mask and etch). For example, alkane thiols were leveraged as templates both for carbon nanotubes (CNTs) (Wang *et al*. 2006; Zou *et al*. 2007) and for viruses (Vega *et al*. 2007). Alkane thiols were further leveraged as an etch-resist layer (Salaita *et al*. 2006a; Zhang *et al*. 2003, 2004; Zhang *et al*. 2007), thereby enabling a rapid method for creating metallic nanostructures. Alongside this evolving palette of inks, ink delivery methods were developed to enable combinatorial DPN patterning with different inks on different tips (Sekula *et al*. 2008), wherein microfluidic inkwells deliver the desired ink solutions to sets of tip-sized microwells that are pitch-matched to the cantilever array. Concurrently, one-dimensional (1D) arrays of DPN probes were developed to both enable this multiplexing and increase overall throughput (Salaita *et al*. 2005). To provide addressable directed placement without cross-contamination, actuated cantilever arrays were developed using thermal bimorph technology (Bullen *et al*. 2004); we now achieve *Z*-actuation ranges greater than 30 μm at temperatures that are within the safe operating ranges for most biomolecules (ActivePens^{TM}; NanoInk, Skokie, IL). Comprehensive discussions of these and other advances can be found in the noted review articles (Ginger *et al*. 2004; Haaheim and Nafday 2008; Huck 2007; Lenhert 2008; Rosner and Demers 2005; Salaita *et al*. 2007).

All of these advances are now incorporated as commonplace methods in the overall DPN toolkit. But more recently, two-dimensional DPN (2D-DPN) has emerged as a viable and robust large-area patterning method while maintaining DPN's nanoscale feature sizes (Haaheim and Nafday 2008; Lenhert *et al*. 2007; Salaita *et al*. 2006b). Scanning Probe Lithography (SPL) has witnessed a dramatic transformation with the advent of these 2D probe arrays. Outside the realm of direct deposition, a key preceding example of massively parallel 2D arrays of nanoscopic tips was the "millipede" (Vettiger *et al*. 2000); however, this device was limited to destructive patterning involving polymer thermal indentation and annealing. Although early DPN work with single probes was justifiably assessed as being too slow to practically apply in a nanomanufacturing context, we have demonstrated throughputs up to $3 \times 10^7\,\mu m^2/h$—in some cases exceeding EBL—using centimeter square arrays of 55,000 tips tailored for DPN. Parallelizing DPN has been critical because there exists a need for a direct deposition lithographic process that is not only high throughput, but also high resolution with massive multiplexing capabilities. In 2006, Salaita *et al*. (2006b) conclusively showed that DPN could be simultaneously performed with 55,000 tips across a square centimeter. With throughput exceeding $1 \times 10^7\,\mu m^2/h$ and a dot size standard deviation of only 16%, they demonstrated sub-100 nm massively parallel nanoscale deposition and patterned an image of the Jefferson nickel. The patterned octadecanethiol (ODT) served as an etch resist on the gold layer, which was imaged optically. They also used these DPN-generated thiol templates to create fibronectin arrays. Initial challenges included 2D planar surface alignment, which was overcome through a combination of taller tips and an epoxy–resin-based self-leveling technique. In 2007, Lenhert *et al*. extended these methods to the phospholipid 1,2-dioleoyl-sn-glycero-3-phophocholine (DOPC). They were able to pattern complex features at an astounding throughput of $3 \times 10^{10}\,\mu m^2/h$, and showed that DOPC can be used as a universal ink for non-covalent patterning on silicon, glass, titanium, and hydrophobic polystyrene, with lateral resolution down to 100 nm. Generally, phospholipids are an essential component of biological membranes and arrays of them can be used as cell-surface models; high-resolution DPN patterning creates model systems capable of mimicking the structural complexity of biological membranes and provides a singularly unique method to generate heterogeneous, multivalent, planar supported lipid bilayers covering large areas with feature sizes smaller than a single cell.

Despite the impressive results described earlier, several engineering difficulties remained with the devices used by these groups. Significant challenges still included leveling the array with respect to the substrate and ensuring uniform contact of all of the tips when the array is meant to write. Either of these scenarios can result in non-uniform patterning or possible cantilever damage. At that time, there was no way to see a clear image of the substrate through the 2D array—patterning amounted to "flying blind." Furthermore, our collaborators' method for mounting the devices on the instrument involved setting the device on the

sample surface (where it was naturally level), and then bringing the scanner in contact with the device with a small blob of epoxy in between. However, the epoxy takes >1 h to cure and can introduce volume distortion that will affect the leveling. Additionally, if multiplexed ink delivery methods are used to address different inks to different tips, the surface contact time will introduce cross-contamination. We have previously reported (Haaheim and Nafday 2008) on the development and implementation of the commercially available 2D nano PrintArray inasmuch as that device solved the problems related to mounting, leveling, and substrate viewing: we introduced etched viewports, a precisely machined magnetic wedge, and highly curled cantilevers for 15+μm freedom of travel (FOT). This enabled us to measure planarity offsets by examining cantilever deflection through these viewports at three different points, noting the *z*-height differences, and then using software routines to calculate and execute planarity with the three *z*-motors. However, those methods still incorporated non-trivial user manipulation to bring the array level to the substrate and achieve sufficient planarity to get all of the nanoscopic tips touching evenly. With the goal of practical implementations of DPN for nanomanufacturing, we sought to automate these printing processes to the greatest extent possible.

In this article, we demonstrate a self-leveling fixture for the 2D nano PrintArray. When mounted on NanoInk's NLP 2000, the 55,000 tip array can achieve a planarity of $<0.1^\circ$ with respect to the substrate in a matter of seconds, with no user manipulation required. Additional fine-leveling routines can improve this planarity to $<0.002^\circ$ with respect to the substrate—a *Z*-difference of <600 nm across 1 cm^2 of surface area. We, herein, show highly homogeneous etch-resist nanostructure results patterned from a self-leveled array of DPN pens. We illustrate the mechanisms and methods of the operating self-leveling fixture, and detail the advantages thereof. Finally, we emphasize that this methodology brings us closer to the goal of true nanomanufacturing by automating the leveling process, reducing setup time by at least a factor of 10, enhancing the ease of the overall printing process, and ultimately ensuring a more level device with subsequently homogeneous nanostructures.

Materials and Methods

We used the 2D nano PrintArray devices as commercially available (NanoInk). The self-leveling fixture was developed internally and is now commercially available. Before patterning, we vapor-coated the 2D tip arrays with ODT, according to three coating cycles: 60 min at 65°C and 100 min cool down at 0.1°C/min. We performed the patterning on the NLP 2000 (NanoInk), which we also used for capturing optical images of cantilever deflection behavior. We performed patterning in ambient conditions (22°C, 30% Rh). Post-patterning, we etched the substrate to create metallic nanostructures, according to the published methods (Salaita *et al.* 2006). We obtained scanning electron microscope images with a Hitachi S4800 SEM Tokyo, Japan. We obtained bright field and dark field optical images with a Zeiss Axio-Imager Z1M Thonrwood, NY.

Results and Discussion

Figure 1(A) illustrates the basic concept of multiplexed 2D-DPN—all tips necessarily draw the same shapes at the same time but each tip can be loaded with different ink. A small water meniscus is shown to represent the natural meniscus that forms between the tip and substrate in ambient conditions, and which is a vehicle for diffusion among classes of diffusive inks (e.g., alkane thiols). Figure 1(B) narrows this idea to multiplexed printing of proteins, envisioning a rapid prototyping platform for creating tailor-made assay kits. In this idealized

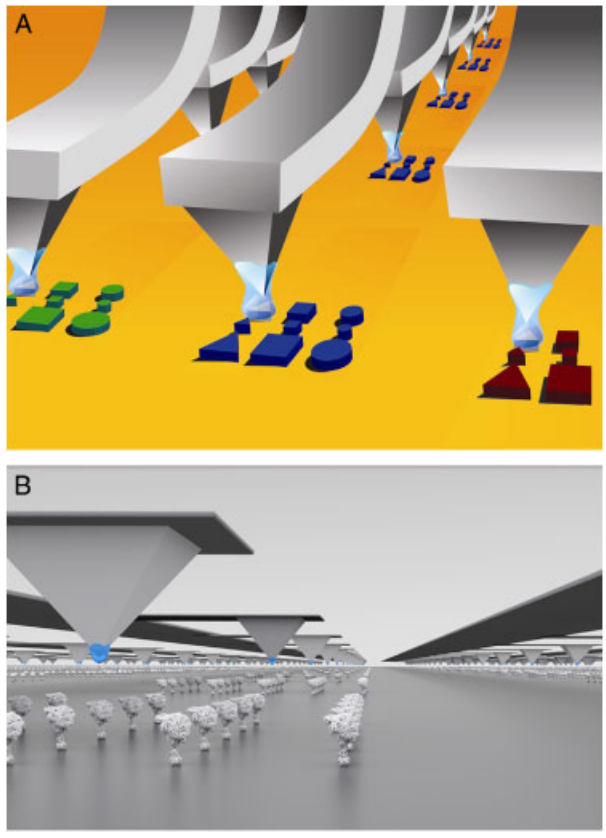


Fig 1. (**A**) Schematic of multiplexed 2D-DPN. (**B**) Idealized schematic of a rapid prototyping platform for multiplexed protein printing.

case, the protein molecules are shown deposited with uniform orientation—a goal of high-throughput DPN printing but acknowledged as a current shortcoming and an area of ongoing development. Nevertheless, each scene serves to illustrate the concept of many thousands of cantilevers hovering just above the surface, all needing to be brought into contact with the substrate gently and uniformly.

This concept—controlled and uniform contact—is the focus of this article in terms of optimizing 2D-DPN. Traditional DPN with single tips or 1D arrays can be performed in force-feedback, with a laser bouncing off the cantilever and onto a photodetector to facilitate a constant applied force (i.e., cantilever deflection) with respect to the substrate. Due to the nature of mechanical amplification on an AFM, the range of cantilever deflection achievable in force-feedback is necessarily constrained by the dimensions of the photodetector; this cantilever deflection range is usually less than 2 μm. By contrast, 2D-DPN is performed without force-feedback, where the *Z*-actuator is set at a constant height with respect to the substrate. Within the range of force-feedback conditions, DPN is effectively force independent, and patterns are created nearly identically between minimum and maximum deflections. However, in situations of extreme tip deflection (e.g., more than 10 μm), we have observed anomalous patterning behavior, including skewed features and non-standard formation of self-assembled monolayers (SAMs). This implies two very important operating conditions for creating uniform and homogenous patterns with 2D-DPN: (1) the overall *Z*-position of the 2D array must be carefully controlled with respect to the substrate (i.e., cantilever deflection average), and (2) the variation in cantilever deflection must be minimized (i.e., cantilever deflection variance, which is directly linked to array-substrate planarity). As we will show, the improved optics of the NLP 2000 make ♯1 far easier to achieve; the self-leveling fixture greatly improves the ease of achieving ♯2 while simultaneously enabling unprecedented planarity.

Beginning with the 2D nano PrintArray itself, Figure 2(A) shows a top view of the silicon chip attached to a redesigned plastic handle. The handle is symmetric along the *x*-axis, with a large cutout in the middle to allow maximum light admission and viewing range for the chip's viewports. The viewports are arranged in a "Y," such that one can make measurements from any of the legs of the "Y" to define the three points of contact with the substrate. Figure 2(A) also shows the inset spherical ball magnets, which are used to attach the 2D nano PrintArray to the rest of the fixture. For convenience, storage, and transport, flat disk magnets are provided in the outer portion of the handle to allow the device to be safely attached to any magnetically permeable material; the device is shown suspended on its left side from the underside of a magnetically permeable metal tin. Figure 2(B) provides a perspective of the same setup from below; the "Y" configuration of the viewports are visible as tiny slits of light coming through the top of the chip. Figure 2(C) shows the inner three viewports (1a, 2a, 3a) explicitly. In this orientation, the ODT-coated tips are pointed toward the viewer, and density of the cantilever packing is shown according to their 20×90 μm pitch arrangement. The viewport width allows viewing 1 row of 13 adjacent cantilevers simultaneously; this greatly aides navigating to the substrate in *Z*, and across it in *X* and *Y*. The silicon nitride (SiN) cantilevers appear green in front of the green–yellow backdrop of the silicon handle wafer, and the pink areas of SiN provide the anchor to the handle. This arrangement is seen explicitly in Figure 2(D): the rows of SiN cantilevers are attached to the ridges of the silicon handle wafer via a gold thermocompression bond. The areas underneath the cantilevers are etched away to provide maximum cantilever deflection. Figure 2(E) zooms in on a group of cantilevers in front of the 260-μm wide viewport aperture, whereas Figure 2(F) indicates the large FOT (typically 15–20 μm) available to each cantilever because of its high curl and the etched-away area beneath it. Solid SiN standoffs (4-μm height) are located at the outer corners of the device; these prevent the cantilevers from ever becoming fully deflected. All tips are fabricated according to standard oxide sharpening processes, resulting in tip sharpness ~15 nm (end radius).

The FOT available to the cantilevers directly defines the minimum allowable planarity to get all of the tips in contact with the substrate. Figure 3(A) shows a schematic of the array just before making contact with the surface, where the array is at the minimum angle (φ). The difference between the highest and lowest part of the array (ΔZ) is the same as the difference between the highest and lowest tip—19.5 μm. As the array moves toward the substrate, the tips on the right will begin deflecting in the order shown, moving left, until the leftmost tip just barely touches the surface. This happens simultaneously as the rightmost standoff touches. Figure 3(B) illustrates why large FOT cantilevers make the leveling process more forgiving. Figure 3(B) also illustrates that to minimize the variance in cantilever deflection across the array, it is necessary to minimize φ and make the device as planar as possible.

Planarity is accomplished using the self-leveling fixture. The operating concept is that a fixture with two orthogonal axes of rotation (φ_x, φ_y) will

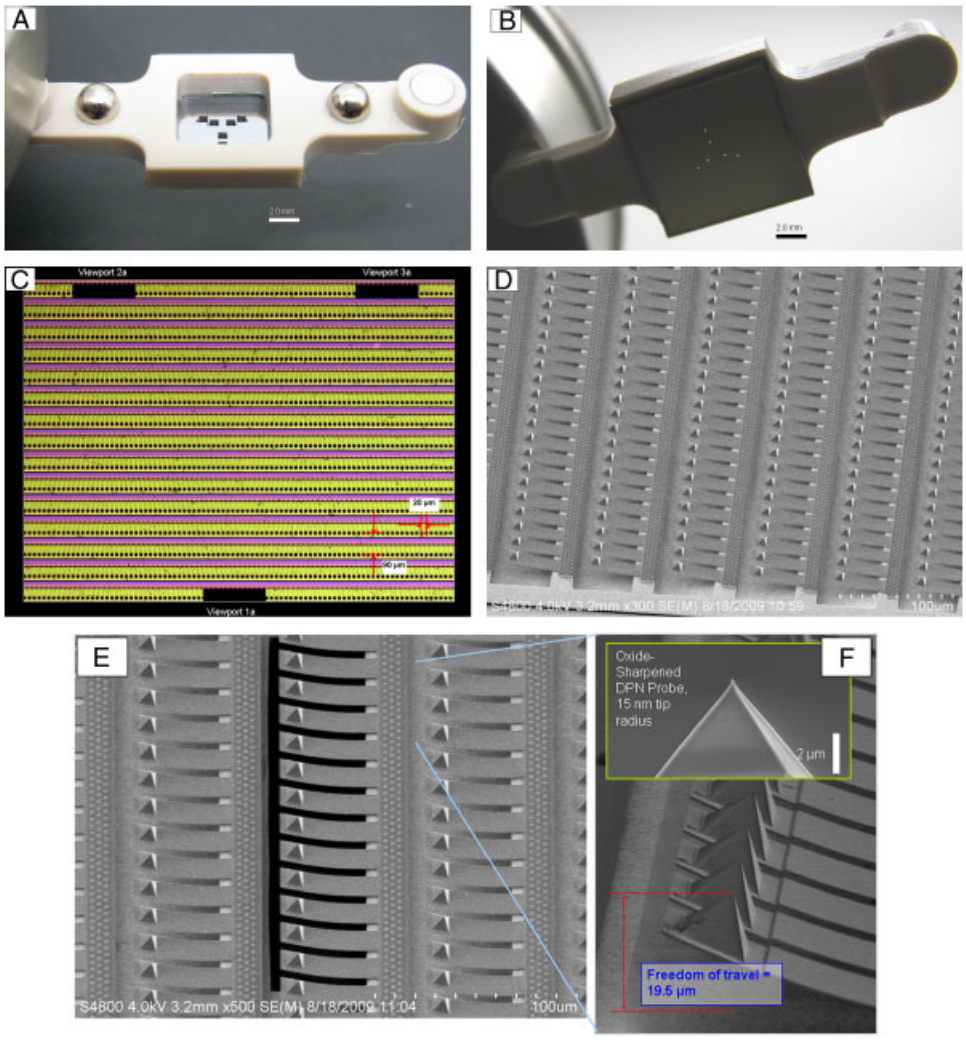


Fig 2. (**A**) Top view of the 2D nano PrintArray mounted to the self-leveling handle. (**B**) Bottom view of the 2D nano PrintArray. (**C**) Optical microscope image of the tips and cantilevers showing their arrangement and pitch, and the placement and size of the viewports. (**D**) SEM image of the tips and cantilevers showing the underlying structure that permits their freedom of travel. (**E**) Zoomed SEM image of the cantilevers in front of a viewport. (**F**) SEM image of the cantilever's freedom of travel.

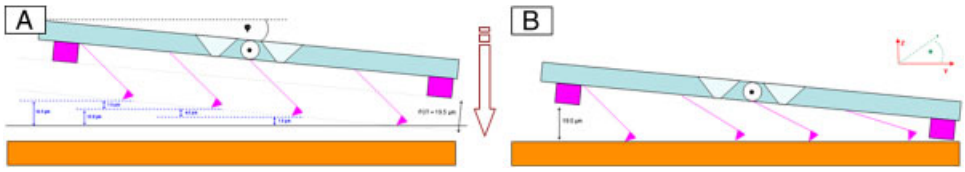


Fig 3. (**A**) Schematic of 2D nano PrintArray just before making contact with the minimum allowable planarity to get all of the tips touching. (**B**) All of the tips are in contact, but the standoff on the right side of the device is also touching the substrate; φ needs to be minimized to achieve the best planarity and subsequent patterning homogeneity.

accommodate the planarity of anything it physically encounters; with the 2D nano PrintArray, this occurs when all four SiN corner standoffs contact the substrate. Figure 4(A) shows how all of the components fit together. The fixture consists of three main components: the top mount which is attached to the rigid probe-holder fixture, the middle gimbal, and the bottom handle which is glued to the 2D nano PrintArray. There are two points of contact between the middle and the top: the fixed spherical magnetic balls attach via a two-point kinematic mount to an inverted cone and a groove, both of which are magnetically permeable and have magnets mounted behind them. Similarly, there are two equivalent kinematic mount points of contact between the handle and the middle. The spherical balls that are fixed in the handle rotate freely along φ_x in their mounts, and the balls fixed in

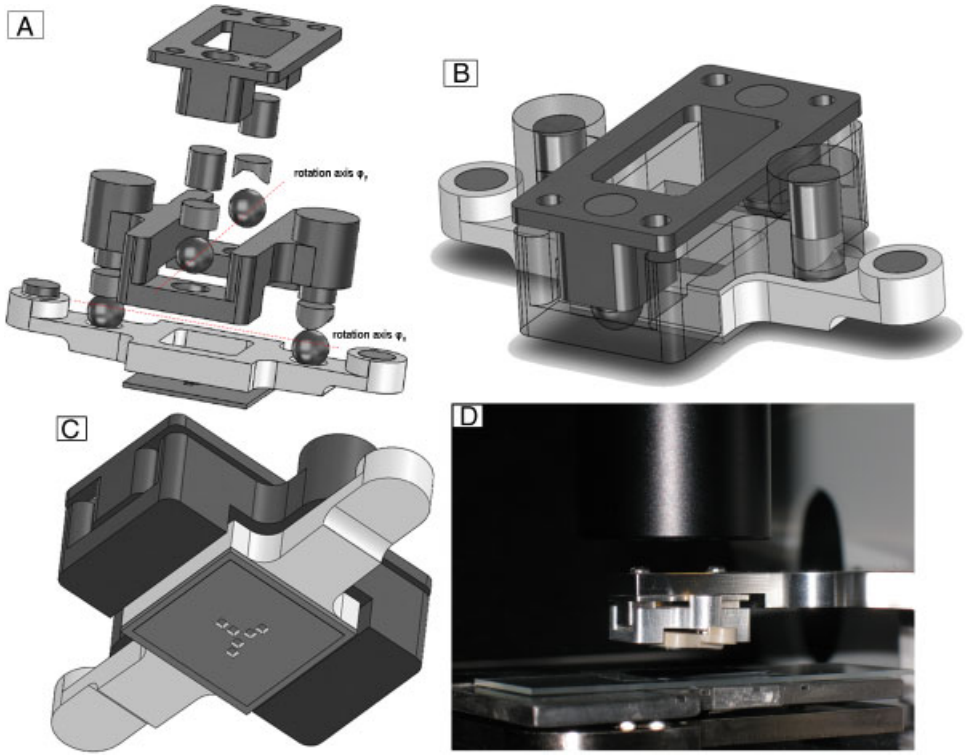


Fig 4. (**A**) Schematic showing how all of the self-leveling fixture components fit together. (**B**) Transparent schematic of the assembled components. (**C**) Opaque bottom view of the assembled components. (**D**) Picture of the real device assembled, mounted, and in use.

the middle piece rotate freely along φ_y. (We note that this self-leveling fixture is not functionally limited to only centimeter square arrays of cantilevers and tips; the generality of its design permits a variety of small-scale device leveling operations.) The magnet strength is calibrated to be weak enough to allow φ_x–φ_y rotation compensation to match the substrate planarity when the standoffs touch down, but strong enough to hold that precise planar orientation for all subsequent operations. Figure 4(B) shows a transparent schematic of the device as it would actually be assembled, and Figure 4(C) illustrates the same assembly from the underside where the exaggerated viewports are shown. Finally, Figure 4(D) shows the real device as actually mounted; the 2D nano PrintArray and its handle are intentionally tipped forward along φ_x to illustrate the ranges of movement.

From this point, the leveling process is very straightforward: one views the cantilevers through the viewports and brings the substrate upward in Z until it meets the first corner of the device, whereafter it self-levels as the cantilevers fully deflect. The cantilever deflection behavior can be seen in Figure 5(A and B); the cantilevers undergo a dramatic optical change indicative of surface contact. Maximizing this deflection correlates to making contact with all of the standoffs, and the device is then self-leveled. This is considered the ''coarse-leveling'' step.

''Coarse-leveling'' is a relative term, however. Figure 6(A) shows a representative schematic of the ''coarse-level'' situation. In this case, we determined the contact points at the viewports (1b, 2b, 3b) according to the deflection behavior shown in Figure 5(A and B). Notably, the clarity of the system optics allows us to determine that point-of-contact to within ± 100 nm so that we can know how good our ''coarse-leveling'' actually was. There are several optical indicators that enable that degree of precision: most prominently, the red–orange refracted light ''butterfly wing'' formation inside the pyramidal tip (Fig. 5(A)) changes shape and color dramatically as soon as the tip's position changes (in Z, tip, or tilt). The apparent color and intensity of the cantilever body will also change. The ease and clarity of these measurements enables us to minimize surface contact time with these inked tips; alternatively, one can level the device in a sacrificial substrate area, and then translate 1 cm to the designated clean patterning area. At all times, the measurements are made by quickly actuating and retracting the Z-stage, noting whether the expected optical indicators manifested at that particular viewport. In Figure 6(A), these point-of-contact measurements yield a set of three Z-coordinates

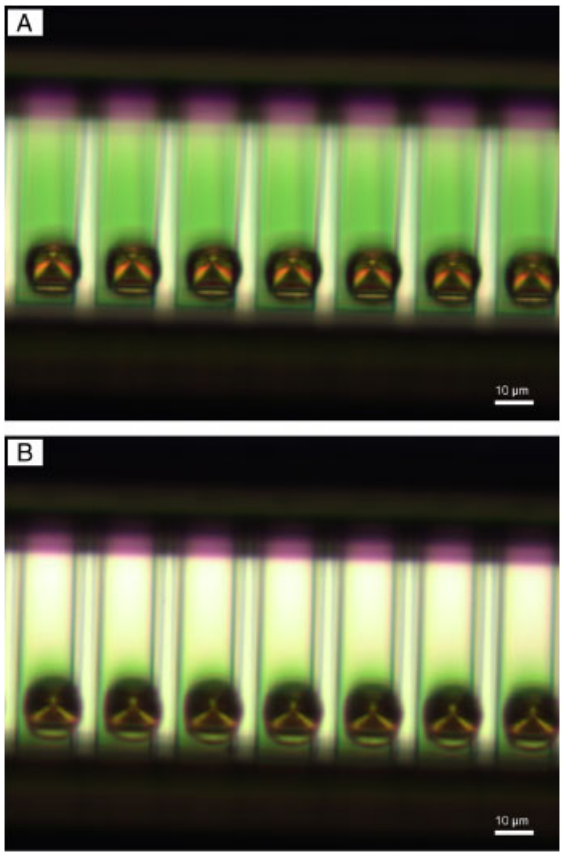


Fig 5. (**A**) Optical image of the 2D nano PrintArray cantilevers as seen through a viewport. The tips are hovering 1 μm above the substrate, just before making contact. The red-orange refracted light "butterfly wing" formation inside the pyramidal tip has not yet undergone the change indicative of substrate contact. (**B**) Cantilevers are fully deflected, indicating that the corner standoffs are uniformly touching. The "butterfly wings" have commensurately changed shape, color, and intensity.

(−539.0, −539.1, and −537.4) that describe the device's planarity; the software calculates the corresponding "slope" (φ) and ΔZ using the device dimensions. Figure 6(A) shows these measurements taken immediately after coarse-self-leveling: with a slope of 0.038° and $\Delta Z = 9.8$ μm, the "coarse level" result is actually very good. Not only is it as good as the best we could get with previous methods—wherein the ΔZ falls within the cantilever FOT ($\Delta Z = 9.8$ μm $<$ FOT $= 19.5$ μm), indicating that all of the tips can be touching—it is also below the extreme tip deflection limit (10 μm). If desired, we could have begun patterning immediately and achieved relatively homogeneous results.

However, this situation naturally lends itself to a "fine-leveling" step. Using the measured Z-coordinates from Figure 6(A), the system can automatically adjust the φ_x–φ_y stages to correct for the slight measured misalignment ("Execute Leveling"). Figure 6(B) shows the results measured immediately after the fine-leveling step: the slope of 0.002° and $\Delta Z = 600$ nm correspond to the cantilever deflection detection limit of ± 100 nm. The device was as planar as could be measured with these methods. For scale comparison, $\Delta Z = 0.6$ μm across the device width of 10,000 μm is equivalent to 5 mm of ΔZ along the length of a football field. With the variation in cantilever deflection minimized (i.e., the device being extremely level), it was then trivial to observe cantilever deflection at one viewport to calibrate the array's overall Z-position with respect to the substrate. (We determined cantilever deflection of 2 μm past the first contact point to be optimal.) Having satisfied the two important operating conditions for homogeneous patterning,

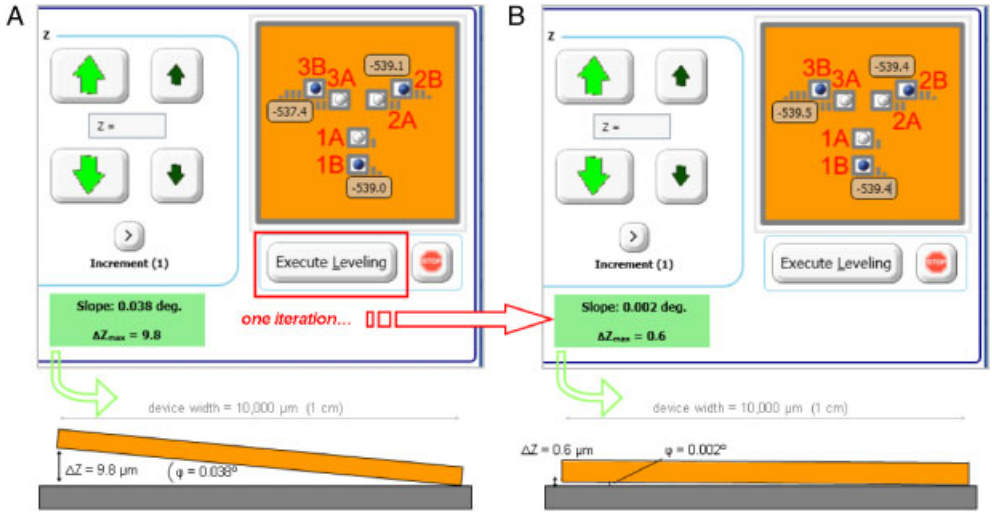


Fig 6. (**A**) NLP 2000 software interface showing the point-of-contact measurements made at viewports 1b, 2b, and 3b immediately after coarse-self-leveling. Upon using the "Execute Leveling" command, the system adjusts the φ_x–φ_y stages to compensate for the planar misalignment, and we immediately re-measured the point-of-contact measurements shown in (**B**). The slope of 0.002° and $\Delta Z = 600$ nm correspond to the cantilever deflection detection limit of ± 100 nm, which means that the device was as planar as could be measured with these methods.

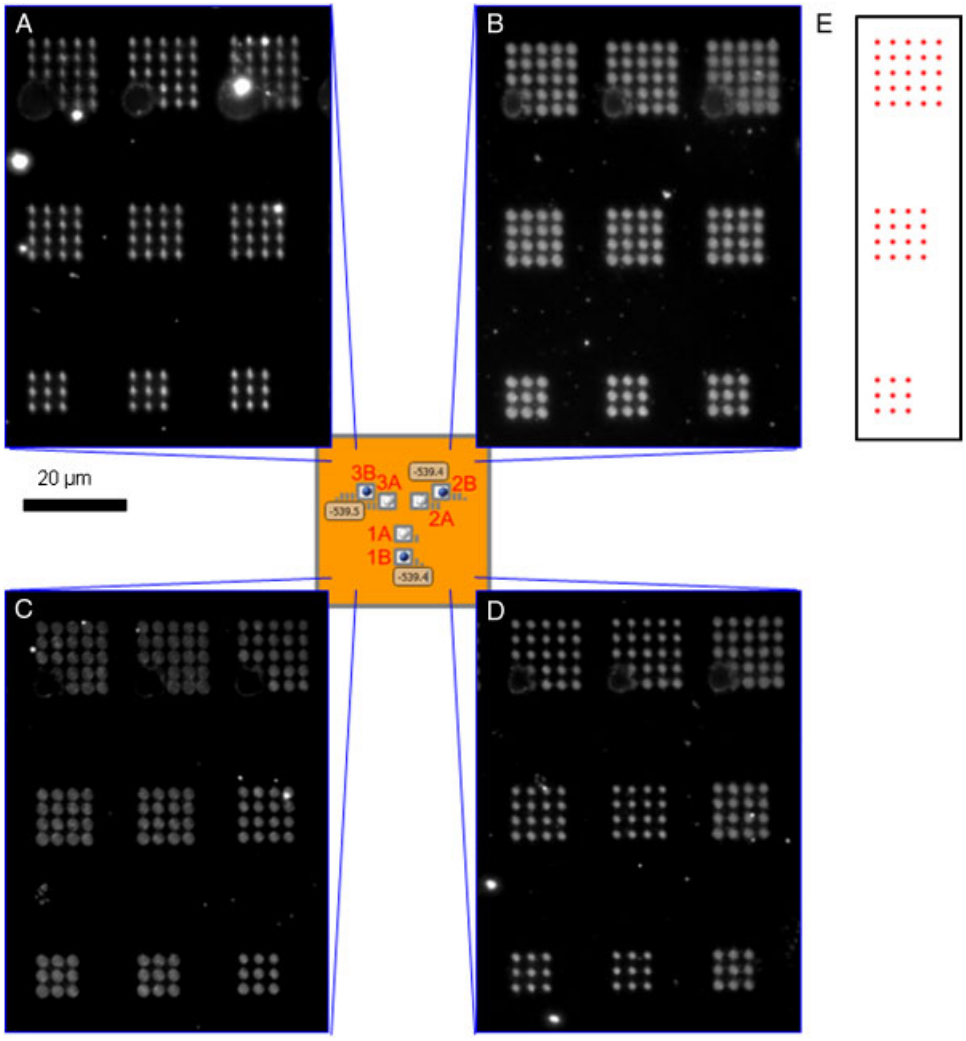


Fig 7. (**A**) Top left, (**B**) top right, (**C**) bottom left, and (**D**) bottom right dark field microscopy images from the homogeneous cm^2-area pattern generated from the Figure 6 printing conditions. The dots are 3-µm pitch with 2-s dwell time, and are 15-nm thick gold structures on a SiO_2 substrate. (**E**) The NLP 2000 software-generated pattern design.

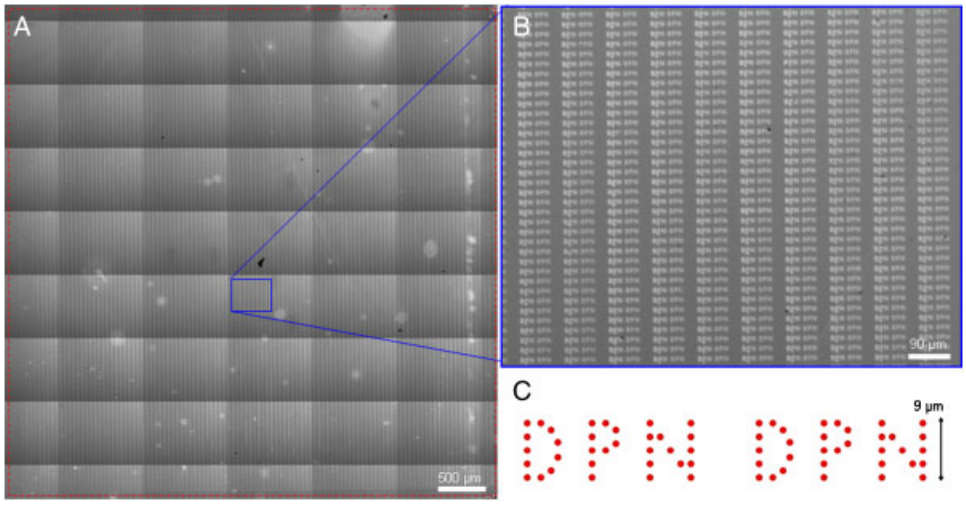


Fig 8. (**A**) Tiled bright field microscopy images illustrating pattern homogeneity across the entire square centimeter, with feature size standard deviation < 6%. (**B**) Zoomed area showing the "DPN DPN" result uniformity from the software design (**C**).

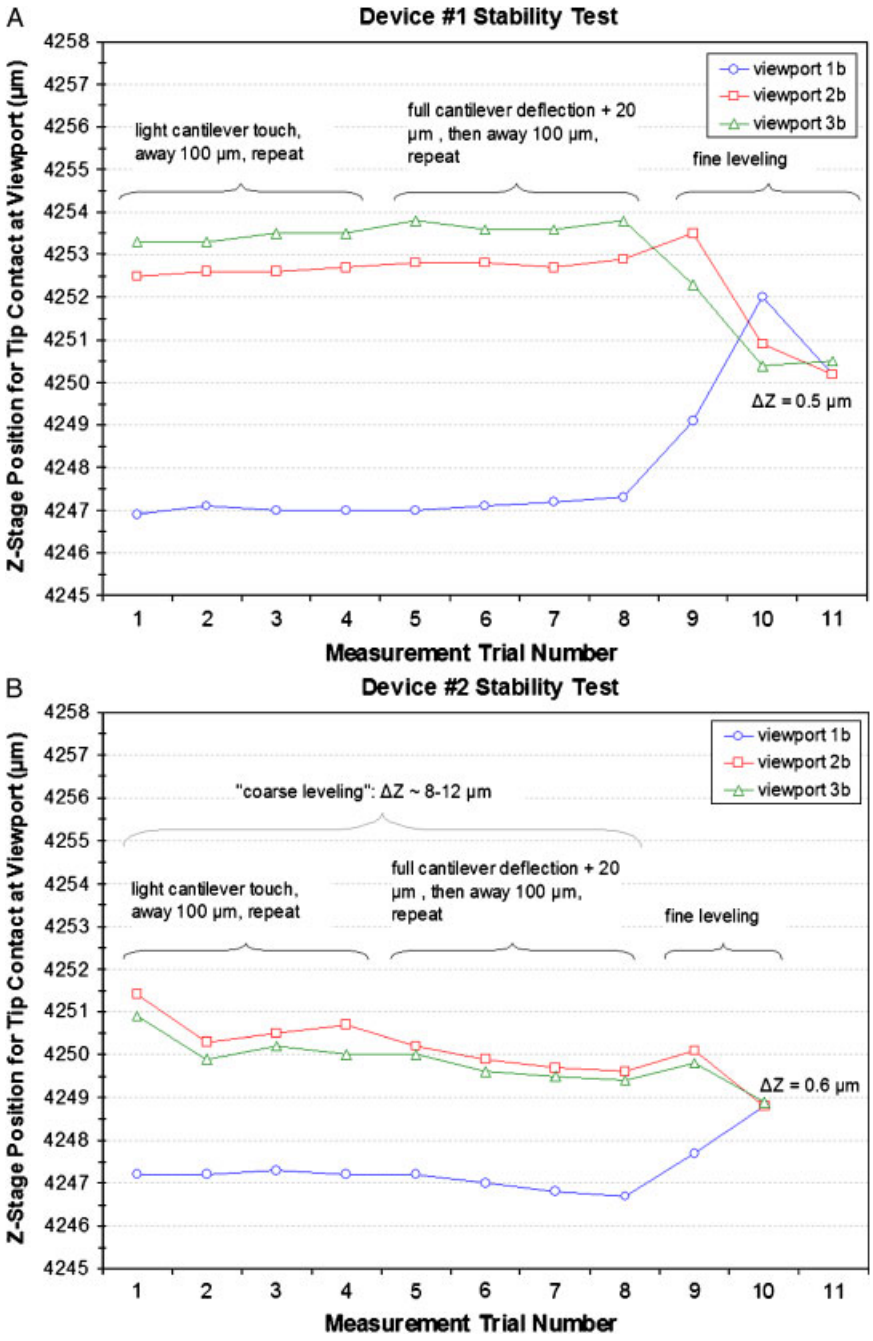


Fig 9. Two sets of self-leveling-fixture stability data show both that the absolute *Z*-positions of the viewports remain constant and that their relationship to each other remains fixed during self-leveling operations. This confirms that the strength of the magnets maintains the device's planar orientation after self-leveling. (**A**) Device ♯1 has a unique angular resolution as shown by the viewport spread. This is because of the unique material interface between the spherical magnetic ball and its kinematic mount. (**B**) A slightly different angular resolution and material interface is seen for device ♯2, but both are well within reasonable working limits.

our subsequent results confirmed the expected homogeneity (Figs. 7 and 8).

Figure 7(A–D) displays the dark field microscopy images obtained from the four corners of the overall centimeter-square pattern, as dictated by the software design input (Fig. 7(E)). The dot dwell times were 2 s, and the dot pitch was 3 µm. The dark field images show 15-nm thick gold structures on an SiO_2 substrate, with strong uniformity between the four corners. The large spot in the bottom left corner of the 5×5 array was formed by dwelling on the substrate for several seconds before initiating patterning. Figure 8(A) speaks to the overall uniformity across the entire square centimeter, with

56 bright field microscopy images tiled together to illustrate the consistency across the sample. In our collaborators' work discussed earlier (Salaita *et al.* 2006), they previously measured a feature size standard deviation of 16% across a centimeter square sample; our current work (Fig. 8(A)) shows 5.4% standard deviation of feature size across the centimeter square sample, with measurements taken from all 56 image tiles. The central portion of the overall pattern is expanded in Figure 8(B), revealing a new pattern based on the "DPN DPN" design from Figure 8(C). (The dwell time for each dot was 20 s.) This level of homogeneity in printing from 55,000 tips is extremely difficult to achieve without appropriate leveling techniques. The self-leveling fixture makes it fast and easy.

Figure 9(A and B) illustrates the self-leveling fixture's ability to maintain its arrived-at planarity across multiple lithography runs. The stability tests for self-leveling fixture ♯1 are shown in Figure 9(A) and are a direct result of the precisely-calibrated magnet strength: if the magnets were too weak, the device would not be able to maintain the planar consistency in trials 1–8. In this experiment, the first four trials involved bringing the array into contact with the substrate, measuring the points of contact for the viewports (1b, 2b, 3b), withdrawing 100 μm, and repeating. Trials 5–8 involved bringing the array into contact with the substrate, moving 20 μm past full cantilever deflection, and then withdrawing 100 μm. The consistency of measured viewport positions means that the self-leveling fixture adopts a very stable orientation regardless of subsequent amounts of cantilever deflection. However, the discrepancy between viewport contact points is itself an indirect measurement of the self-leveling fixture's angular resolution, which is in turn representative of the material interfaces between the spherical magnetic balls and their kinematic mounts. Trials 9–11 show the beginning of the fine-leveling steps, leading to the expected minimized ΔZ (0.5 μm). Figure 9(B) shows the same behavior with a second device–fixture ♯2. This device shows the coarse-leveling results noted above ($\Delta Z \sim 8$–12 μm), and similar planar orientation stability. One fine-leveling iteration achieves $\Delta Z = 0.6$ μm. The slightly different viewport spread seen in Figure 9(B) results from a slightly different ball-mount material interface due to machining and polishing variations that are within normal tolerances.

Conclusion

We have demonstrated a self-leveling fixture for 2D-DPN patterning that greatly minimizes the time required to level the device, simplifies the leveling procedure, and provides much better co-planarity than was previously achievable. Fine-leveling routines can result in $<0.002^\circ$ misalignment with respect to the substrate—a Z-difference of less than 600 nm across 1 cm^2 of surface area. The degree of planarity directly correlates to homogeneity, which determines patterning quality across large areas. The ease and precision of this method enhances access to three categories of 2D nanopatterning applications mentioned above: (1) rapidly and flexibly generating nanostructures (e.g., Au, Si) via etch-resist techniques; (2) chemically directed assembly and patterning templates for either biological molecules (e.g., proteins, viruses, and cell adhesion complexes), or inorganics (e.g., CNTs, quantum dots); and (3) directly writing biological materials. Along with our collaborators, we have patterned both phospholipids and alkanethiols, with thiol functional groups including methyl, hydroxyl, amine, and carboxyl. We can thereby create hundreds of millions of chemically tailored nanostructures in a matter of minutes, with functional groups tailored to specific templating requirements. To date, there is no other way to flexibly pattern a variety of materials at the DPN's resolution (14 nm) across centimeter square areas. Fundamentally, this enables flexible direct-writing with a variety of molecules, simultaneously generating 55,000 duplicates at the resolution of single-pen DPN. By enhancing the speed, ease, and precision of the process, the self-leveling methodology brings us closer to the goal of practical nanomanufacturing.

References

Bullen D, Chung SW, Wang XF, Zou J, Mirkin CA, *et al.*: Parallel dip-pen nanolithography with arrays of individually addressable cantilevers. *Appl Phys Lett* **84**, 789–791 (2004).

Demers LM, Ginger DS, Park SJ, Li Z, Chung SW, *et al.*: Direct patterning of modified oligonucleotides on metals and insulators by dip-pen nanolithography. *Science* **296**, 1836–1838 (2002).

Demers LM, Park SJ, Taton TA, Li Z, Mirkin CA: Orthogonal assembly of nanoparticle building blocks on dip-pen nanolithographically generated templates of DNA. *Angew Chem Int Ed* **40**, 3071–3073 (2001).

Ginger DS, Zhang H, Mirkin CA: The evolution of dip-pen nanolithography. *Angew Chem Int Ed* **43**, 30–45 (2004).

Haaheim J, Eby R, Nelson M, Fragala J, Rosner B, *et al.*: Dip Pen Nanolithography (DPN): process and instrument performance with NanoInk's NSCRIPTOR system. *Ultramicroscopy* **103**, 117–132 (2005).

Haaheim J, Nafday OA: Dip Pen Nanolithography®: a "Desktop Nanofab™" approach using high-throughput flexible nanopatterning. *Scanning* **30**, 137–150 (2008).

Huck WTS: Self-assembly meets nanofabrication: recent developments in microcontact printing and dip-pen nanolithography. *Angew Chem Int Ed* **46**, 2754–2757 (2007).

Lee KB, Lim JH, Mirkin CA: Protein nanostructures formed via direct-write dip-pen nanolithography. *J Am Chem Soc* **125**, 5588–5589 (2003).

Lee KB, Park SJ, Mirkin CA, Smith JC, Mrksich M: Protein nanoarrays generated by dip-pen nanolithography. *Science* **295**, 1702–1705 (2002).

Lenhert S: Materials integration by dip-pen nanolithography in Nanotechnology, Vol. 2—Nanoprobes. WILEY-VCH Weinheim, Berlin (2008).

Lenhert S, Sun P, Wang Y, Fuchs H, Mirkin CA: Massively parallel dip-pen nanolithography of heterogeneous supported phospholipid multilayer patterns. *Small* **3**, 71–75 (2007).

Nafday OA, Haaheim JR, Villagran F: Site-specific dual ink dip pen nanolithography. *Scanning* **31**, 122–126 (2009).

Piner RD, Zhu J, Xu F, Hong SH, Mirkin CA: Dip-pen nanolithography. *Science* **283**, 661–663 (1999).

Rosner BT, Demers LM: Dip pen nanolithography: applications and functional extensions in Dekker encyclopedia of nanoscience and nanotechnology. Taylor and Francis Group, New York (2005).

Salaita KS, Lee SW, Ginger DS, Mirkin CA: DPN-generated nanostructures as positive resists for preparing lithographic masters or hole arrays. *Nano Lett* **6**, 2493–2498 (2006a).

Salaita KS, Lee SW, Wang XF, Huang L, Dellinger TM, *et al.*: Sub-100 nm, centimeter-scale, parallel dip-pen nanolithography. *Small* **1**, 940–945 (2005).

Salaita KS, Wang YH, Fragala J, Vega RA, Liu C, *et al.*: Massively parallel dip-pen nanolithography with 55000-pen two-dimensional arrays. *Angew Chem Int Ed* **45**, 7220–7223 (2006b).

Salaita KS, Wang YH, Mirkin CA: Applications of dip-pen nanolithography. *Nat Nanotechnol* **2**, 145–155 (2007).

Sanedrin RG, Huang L, Jang JW, Kakkassery J, Mirkin CA: Polyethylene glycol as a novel resist and sacrificial material for generating positive and negative nanostructures. *Small* **4**, 920–924 (2008).

Sekula S, Fuchs J, Weg-Remers S, Nagel P, Schuppler S, *et al.*: Multiplexed lipid dip-pen nanolithography on subcellular scales for the templating of functional proteins and cell culture. *Small* **4**, 1785–1793 (2008).

Vega RA, Shen CKF, Maspoch D, Robach JG, Lamb RA, *et al.*: Monitoring single-cell infectivity from virus-particle nanoarrays fabricated by parallel dip-pen nanolithography. *Small* **3**, 1482–1485 (2007).

Vettiger P, Despont M, Drechsler U, Durig U, Haberle W, *et al.*: The ''Millipede''—more than one thousand tips for future AFM data storage. *IBM J Res Develop* **44**, 323–340 (2000).

Wang YH, Maspoch D, Zou SL, Schatz GC, Smalley RE, *et al.*: Controlling the shape, orientation, and linkage of carbon nanotube features with nano affinity templates. *Proc Natl Acad Sci USA* **103**, 2026–2031 (2006).

Wang HT, Nafday OA, Haaheim JR, Tevaarwerk E, Amro NA, *et al.*: Toward conductive traces: Dip Pen Nanolithography® of silver nanoparticle-based inks. *Appl Phys Lett* **93**, 143105-1–143105-3 (2008).

Zhang H, Amro NA, Disawal S, Elghanian R, Shile R, *et al.*: High-throughput dip-pen-nanolithography-based fabrication of Si nanostructures. *Small* **3**, 81–85 (2007).

Zhang H, Chung SW, Mirkin CA: Fabrication of sub-50-nm solid-state nanostructures on the basis of dip-pen nanolithography. *Nano Lett* **3**, 43–45 (2003).

Zhang H, Jin RC, Mirkin CA: Synthesis of open-ended, cylindrical Au-Ag alloy nanostructures on a Si/SiOx surface. *Nano Lett* **4**, 1493–1495 (2004).

Zou S, Maspoch D, Wang Y, Mirkin CA, Schatz GC: Rings of single-walled carbon nanotubes: molecular-template directed assembly and Monte Carlo modeling. *Nano Lett* **7**, 276–280 (2007).